G. HIGH-PRECISION AND HIGH-SENSITIVITY EXPERIMENTS

The powerful and sensitive techniques of nuclear physics can be turned to many fields. Frequently, unique and important results can emerge. This is the case using the Advanced Photon Source at Argonne to investigate, and debunk, claims for "enhanced" decay from hafnium isomers. It is also the case in investigating the concentration of ^{3}He in ^{4}He, an Accelerator Mass Spectrometry (AMS) measurement critical for a new determination of the neutron lifetime.

g.1. Measuring the ^{3}He Content of Ultra-Pure ^{4}He: A Step Toward Determining the Neutron's Half-Life to High Precision

(R. C. Pardo, K. E. Rehm, R. V. F. Janssens, C. L. Jiang, J. P. Schiffer, R. H. Scott, S. Sinha, R. Vondrasek, D. P. Moehs,* C. Bavlsik,† P. Huffman,‡ J. Doyle,§ S. Dzhosyuk,§ D. McKinsey,§ and L. Yang§)

An experiment to determine the fractional concentration of ^{3}He remaining in isotopically purified ^{4}He is ongoing at ATLAS using the technique of Accelerator Mass Spectroscopy (AMS). This measurement is in support of a program to improve the accuracy of the neutron beta-decay lifetime to 1 part in 10^5.

Although we were able to measure the ^{3}He/^{4}He ratio of samples to be $2.6 \times 10^{-13} \pm 1.1 \times 10^{-13}$, the background in the source used would limit the measurements at approximately 1 in 10^{14}. Further improvements in the source background that will allow measurements approaching 1 in 10^{15} are desirable and work to decrease the observed background is in progress. A new source design using pyrolitic boron nitride, in place of quartz, was now tested in an off-line mode and is working well. Beam time to measure the helium background in this new source and the ^{3}He concentration in newly prepared samples is planned for the summer or fall of 2004.

*Fermi National Laboratory, †University of Chicago, ‡National Institute of Standards and Technology, §Harvard University.

g.2. Precision Measurement of the ^{62}Ga Beta-Decay

(G. Savard, B. Lundgren, D. Peng, B. Blank,* A. Blazhev,† G. Canchel,* M. Chartier,‡ J. Doering,† Z. Janas,§ R. Kirchner,† I. Muhka,† E. Roeckl, and K. Schmidt†)

In continuation of the program to extend the set of high-precision superallowed Fermi emitters to heavier systems, we performed a precise measurement of the branching ratio in the beta-decay of ^{62}Ga. The data for this measurement was obtained in September 2002 at the GSI on-line isotope separator. Five large γ-detectors (a cluster detector composed of 7 Ge crystals, 2 GSI clover detectors each containing 4 crystals, and two single crystal detectors), totaling 17 Ge crystals in all, were used for this experiment. The set of γ-detectors surrounded 3 silicon detectors, which were installed around the collection point to detect the emitted βs. A tape transport system was instituted to reduce the effect of long-lived activity. This detector combination was able to yield β-γ, γ-γ, and β-γ-γ coincidences of sufficient quality to allow for the determination of allowed branches to low lying 1^+ states and sufficiently intense non-analog branches to low-lying 0^+ states.

The analysis of this data required the unpacking and recovery of roughly 30 GB of GOOSY files from GSI. A code was written to unpack the data in a format that was acceptable for analysis on the Maria cluster. Much time and effort was then devoted to carefully calibrating the data as well as determining the exact geometry of the detector setup and the effects of the electronic triggers in the data acquisition. We then proceeded in our analysis by investigating possible systematic errors and methods of reducing the background in order to extract the most precise branching ratio measurement from the data.

Although the dominant branch in this decay to ^{62}Zn is the superallowed ($0^+ \rightarrow 0^+$) transition, we found (see

Fig. I-49) that approximately (0.148 ± 0.015)% of the beta decays precede via gamma cascades through the first excited 2^+ state of ^{62}Zn at 0.954 MeV. This result provides a notably higher branching ratio than previously published values (0.120 ± 0.021)%[1,2], although our value remains consistent within error.

The much higher statistics obtained in the September 2002 GSI experiment give convincing credit to our measurement of this branching ratio and furthermore enabled us to make clear observations – and in some cases precision measurements – of approximately 8 other weak Gamow-Teller transitions in this decay. This achievement is significant, considering that nearly all of these lesser branches were unobservable in previous experiments. Among the weak transitions we have succeeded in measuring is a 2.228 MeV γ-ray (Fig. I-50) in strong coincidence with the 0.954 MeV γ-ray. This transition was observed by Blank in 2002[1], yet unconfirmed by Hyman *et al.* in 2003.[2] We find a branching ratio of (0.06 ± 0.02)% for this transition. In addition, we see evidence for population of the ^{62}Zn second 2^+ state at 1.805 MeV, which is given by a 0.851 γ-ray in coincidence with the 0.954 MeV transition. A weakly observable γ-ray is apparent at 1.805 MeV as well, suggesting a direct transition from this 2^+ state to the 0^+ ground state.

We were also able to precisely measure a branching ratio of (0.05 ± 0.01)% for a 1.388 MeV γ-ray (Fig. I-51) in coincidence with the γ-ray at 0.954 MeV, which provides evidence for the population of the first-excited 0^+ state in ^{62}Zn at 2.343 MeV. The branching ratio of this transition, once summed with the other measured forbidden decays, should allow us to determine an upper-limit for the superallowed ($0^+ \rightarrow 0^+$) branching ratio in the decay of ^{62}Ga and yield a direct comparison to the shell model calculations used to calculate isospin mixing corrections in this region.

---

*CEN Bordeaux-Gradignan, France, †GSI, Darmstadt, Germany, ‡University of Liverpool, United Kingdom, §Warsaw University, Poland.

[1]B. Blank, Eur. Phys. J. A **15**, 121-124 (2002).
[2]B. C. Hyman *et al.*, Phys. Rev C **68**, 015501 (2003).

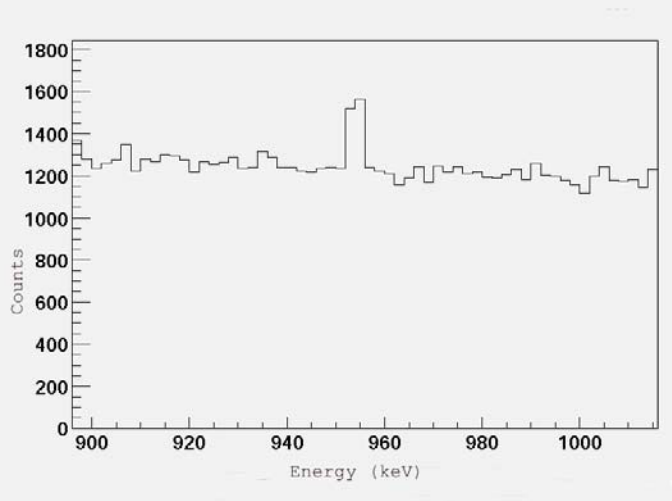

Fig. I-49. β-γ coincidence spectrum in the decay of ^{62}Ga, with counts plotted as a function of energy (keV), showing a strong peak at 0.954 MeV.

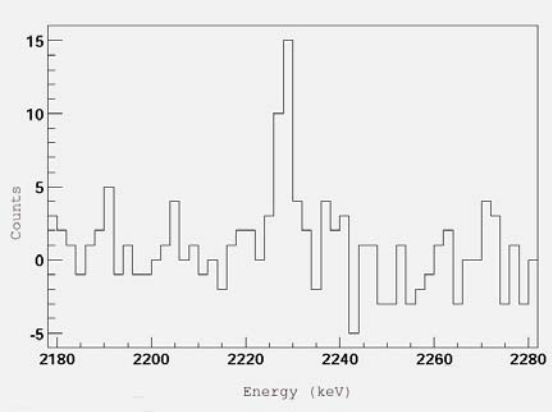

Fig. I-50. A background-subtracted γ-ray spectrum of β and (E_γ = 0.954 MeV) γ-ray coincidences, with counts plotted as a function of energy (keV), revealing a clear peak at 2.228 MeV.

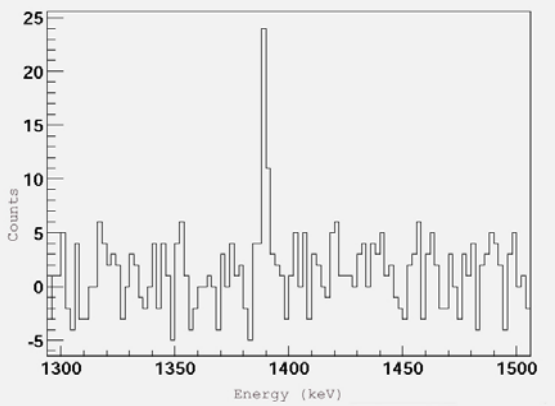

Fig. I-51. A background-subtracted γ-ray spectrum of β and (E_γ = 0.954 MeV) γ-ray coincidences, with counts plotted as a function of energy (keV), revealing a clear peak at 1.388 MeV.

g.3. Search for X-Ray Induced Decay of the 31-yr Isomer of ^{178}Hf at Low X-Ray Energies

(I. Ahmad, D. S. Gemmell, E. F. Moore, J. P. Schiffer, J. Banar,* J. A. Becker,† T. A. Bredeweg,* J. R. Cooper,† A. Mashayekhi,‡ D. McNabb,† P. Palmer,* S. Rundberg,* S. D. Shastri,‡ T. F. Wang,† and J. B. Wilhelmy*)

The search for 'triggered' decay[1] of the 31-yr isomer of ^{178}Hf is the subject of continuing controversy that spilled over into the popular scientific press media.[2] In the past year our group completed a detailed analysis of the experiments carried out at the APS light source with continuous 'white' x-rays irradiating samples of isomeric Hf, results that were reported briefly before.[3] The previous negative results were strengthened and the data were checked for the more recent claims by the proponents of this process for new gamma-ray lines appearing under x-ray bombardment. No such lines were seen. A full paper describing this work was prepared for publication. The final figure is shown in Fig I-52.

*Los Alamos National Laboratory, †Lawrence Livermore National Laboratory, ‡Advance Photon Source, Argonne National Laboratory.

[1]C. B. Collins, *et al*., Phys. Rev. Lett. **82**, 695 (1999); C. B. Collins *et al*., Europhys. Lett. **57**, 677 (2002); C. B. Collins *et al*., Laser Physics **14**, 154 (2004).

[2]New Scientist, August 16, 2003, p. 4; Popular Mechanics, May 2004; Physics Today, May, 2004.

[3]I. Ahmad *et al*., Phys. Rev. Lett. **87**, 072503 (2001); I. Ahmad *et al*., Phys. Rev. C **67**, 041305(R) (2003).

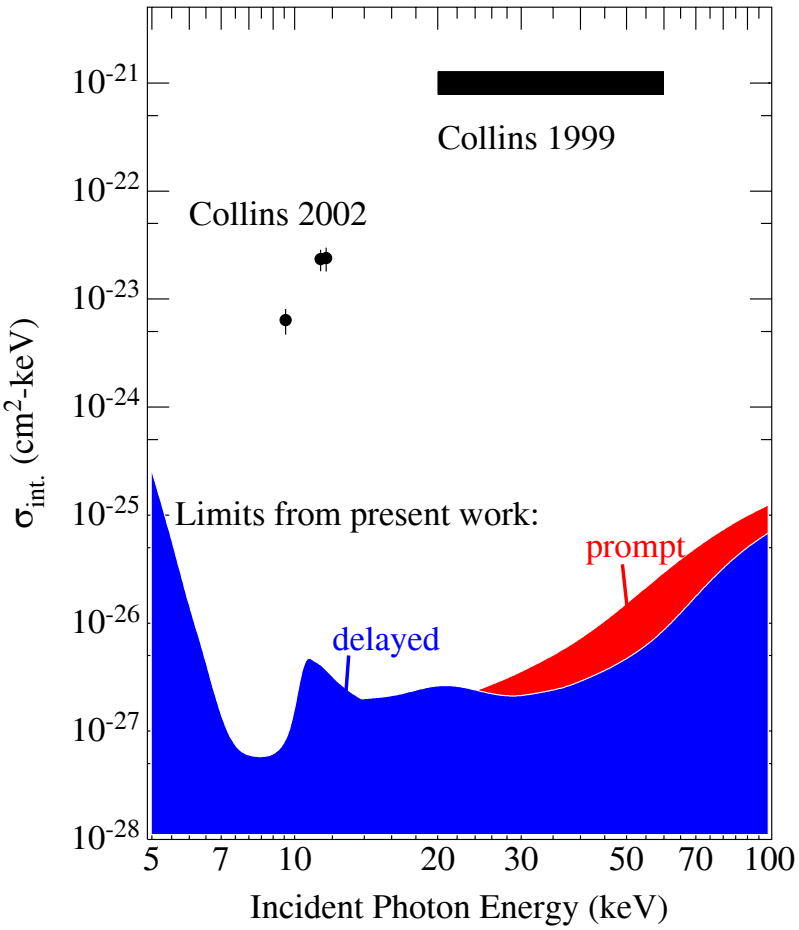

Fig. I-52. Liimiting cross sections (99% confidence limit, including systematic errors) for the cross sections corresponding to all the data in the present measurement for the photon-induced de-excitation of 16+ ^{178m2}Hf isomer. The limits show the combined result for the thick and thin targets. The areas above the colored regions are excluded by the present measurements, with the red area corresponding to the limit for prompt, in-beam de-excitation, and the blue region showing the slightly different limit at high x-ray energies for a delayed one. The values corresponding to the positive results from the measurements of Collins et al. are also shown.

g.4. Calibration of the Beam Energy at ATLAS (C. L. Jiang, K. E. Rehm, I. Ahmad, J. Greene, R. V. F. Janssens, R. C. Pardo, S. Sinha, X. D. Tang, and G. Zinkann)

It was observed that the measured excitation function of fusion-evaporation residues for the system ^{64}Ni + ^{64}N[1] is in good agreement with the results of Ref. 2, but is shifted by about ΔE ~1.5 MeV towards lower energies compared to the results of Ref. 3 at 180 MeV energy region.

In order to verify the beam energy measurement at ATLAS, energy calibration measurements with several heavy-ion beams (^{64}Ni, ^{60}Ni, ^{78}Kr, and ^{16}O), in the energy range of 1 – 10 MeV/u were performed after the ^{64}Ni + ^{64}Ni experiment. The determination of the beam energy at ATLAS is accomplished by using a resonant detection time-of-flight system.[4] Such a system can be referenced to certain "absolute" parameters such as the physical distance between resonant detectors and the electronic delay of signals between various components of the system, which in principle, can be determined independently by other methods.[4] A more precise calibration can be achieved by comparing the time-of-flight with a direct measurement of the magnetic rigidity of the beam. For this measurement an Enge magnetic spectrograph was used, which was calibrated with a strong ^{232}Th α source. The α-energies of this

source, ranging from 5.318 to 8.769 MeV were calibrated with very thin α sources of ^{249}Cf, ^{241}Am, ^{250}Cf, ^{244}Cm, ^{238}Pu and ^{232}Th, whose energies are very well known.[5] The energy spectrum of the strong α source together, with one obtained from a thin ^{232}Th source, is shown in Fig. I-53.

Beams $^{16}O^{6+}$, $^{78}Kr^{16+}$, $^{60}Ni^{14+}$, and $^{64}Ni^{15+}$ extracted from ATLAS were detected with the Enge magnetic spectrograph at 0-degree with and without a ^{197}Au foil, respectively. The measurement results are shown in Fig. I-54, as a ratio between the energy measured with the spectrograph and the time-of-flight system. The beam energy determined by the time-of-flight method at ATLAS agrees well with the value measured with the Enge magnetic spectrograph within the experimental uncertainty. The average ratio of 1.00075 (dashed line) corresponds to a shift of 135 keV at 180 MeV. The largest energy deviation found in these calibration measurements was 0.51%, corresponding to an energy shift 0.92 MeV at 180 MeV, which is smaller than the 1.5 MeV shift mentioned above.

The time-of-flight measurement system for the ATLAS beam energy therefore seems to be very stable (better than 10^{-3}) when compared to the previous calibration[4], which was done in 1987.

[1]C. L. Jiang *et al.*, Physics Division Annual Report 2002, Argonne National Laboratory, p. 85 (2002).
[2]M. Beckerman *et al.*, Phys. Rev. C **25**, 837 (1982).
[3]D. Ackermann *et al.*, Nucl. Phys. **A609**, 91 (1996).
[4]R. Pardo *et al.*, Nucl. Instrum. Methods **A270**, 226 (1988).
[5]A. Rytz, Atomic Data and Nuclear Data Tables B **47**, 205 (1991).

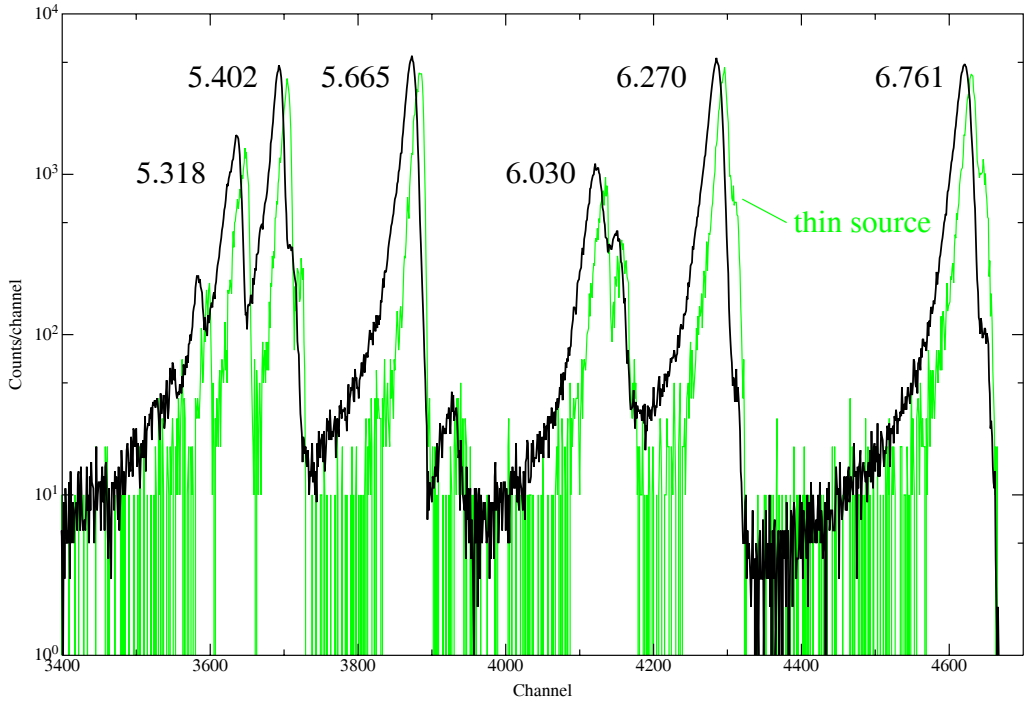

Fig. I-53. Energy spectrum of the strong ^{232}Th α source compared with the spectrum of a thin ^{232}Th α source (thin curve). Numbers indicated are the energies of the peak (MeV). There is another peak at 8.769 MeV outside the plot.

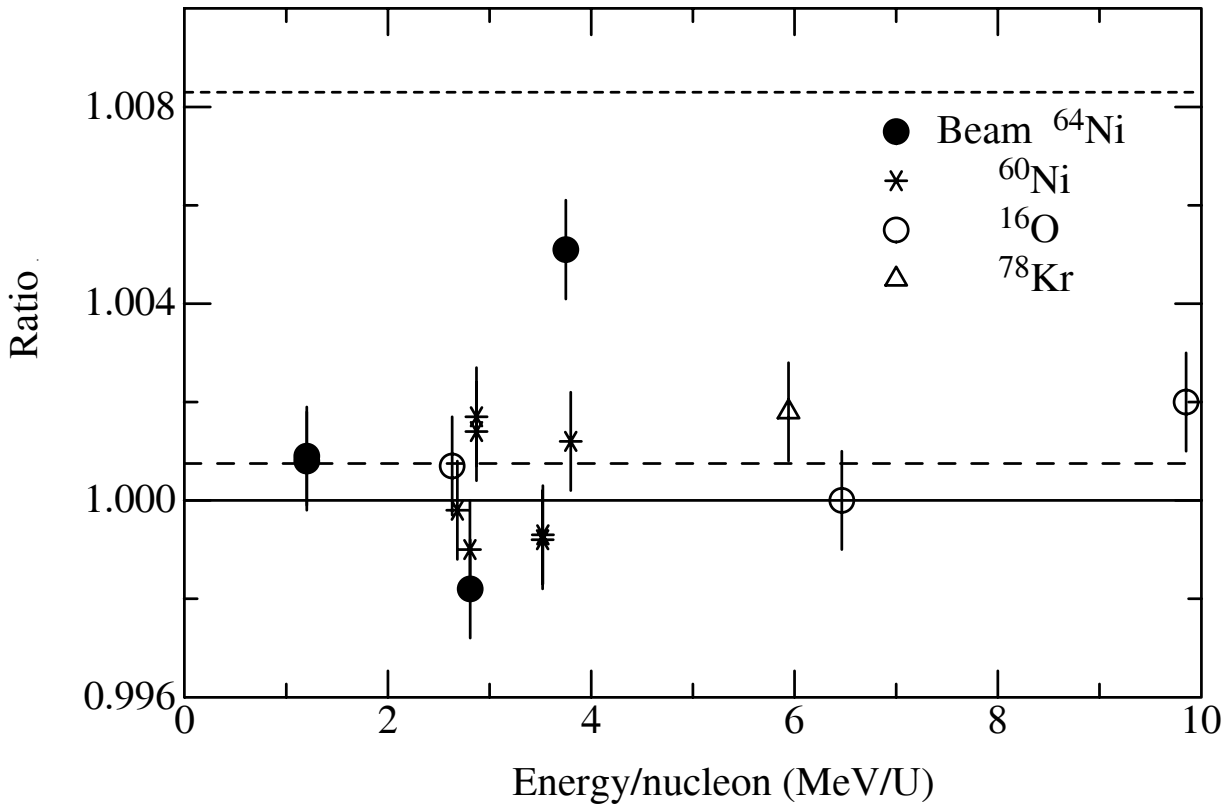

Fig. I-54. A Comparison of the beam energy measurements done with an Enge magnetic spectrograph relative to the time-of-flight system.

g.5. Systematics of Heavy-Ion Fusion Reactions at Extreme Sub-Barrier Energies

(C. L. Jiang, H. Esbensen, B. B. Back, R. V. F. Janssens, and K. E. Rehm)

As mentioned in last year's Annual report[1] the six heavy-ion fusion systems: ^{58}Ni + ^{58}Ni,[2] ^{60}Ni + ^{89}Y,[3] ^{64}Ni + ^{64}Ni,[4] ^{90}Zr + ^{89}Y, ^{90}Zr + ^{90}Zr, and ^{90}Zr + ^{92}Zr[5] were shown to develop a pronounced maximum in the *S* factor at low energies. In addition we found that the energy at which the maximum occurs, coincides with the crossing point between the experimental logarithmic derivative, $L(E) = d(ln(\sigma E))/dE$ and the curve $L_0(E)$ (see Eq. 4 of Ref. 1), which is the logarithmic derivative for an s-wave, point charge, pure Coulomb interaction approximation. In this contribution the systematics for this behavior will be discussed.

The relation between the two representations of the low-energy fusion data, namely, the *S* factor and the logarithmic derivative, can be understood by examining the derivative of the *S* factor, given by:

$$\frac{dS}{dE} = S(E)\left[L(E) - \frac{\pi\eta}{E}\right], \qquad (1)$$

where η is the Sommerfeld parameter $\eta = Z_1 Z_2 e^2 \sqrt{\frac{\mu}{E}}, \mu = \frac{m_N}{2}\frac{A_1 A_2}{A_1 + A_2}$, A_1 and A_2 are the mass numbers of the reaction partners and m_N is the nucleon mass. A maximum in the *S* factor implies that *dS/dE* = 0. This is fulfilled when the logarithmic derivative reaches a value of $L_{CS}(E) = \frac{\pi\eta}{E}$. (2)

This function, which is the logarithmic derivative for a constant S factor, is just as the same as $L_0(E)$ (mentioned above), as long as η is big enough, which is well satisfied for heavy-ion fusion reactions. Let us denote the energy and logarithmic derivative where this intersection occurs by E_s and $L_s = L(E_s)$, respectively. These two quantities are then related by the equation:

$$L_s = \frac{\pi Z_1 Z_2 e^2}{E_s^{3/2}} \sqrt{\frac{m_N}{2} \frac{A_1 A_2}{A_1 + A_2'}} \qquad (3)$$

since they fall on the curve defined in Eq. 2.

Suprisingly, we found that the value of L_s is nearly identical for the six stiff systems, with an average value of 2.34 MeV^{-1}. (See Table I, first six lines in Category I. A recently measured system $^{32}S + ^{89}Y$,[7] also exhibits a well determined maximum in its S factor, which is included in the discussion too.) Assuming that L_s = 2.34 MeV^{-1} is an "universal" value, Eq. 3 can be used to derive an analytic expression for the energy E_s. Thus, inserting the value L_s = 2.34 MeV^{-1} into Eq. 3, we obtain:

$$E_s = 0.355 \left[Z_1 Z_2 \sqrt{\frac{A_1 A_2}{A_1 + A_2}} \right]^{2/3} (MeV). \qquad (4)$$

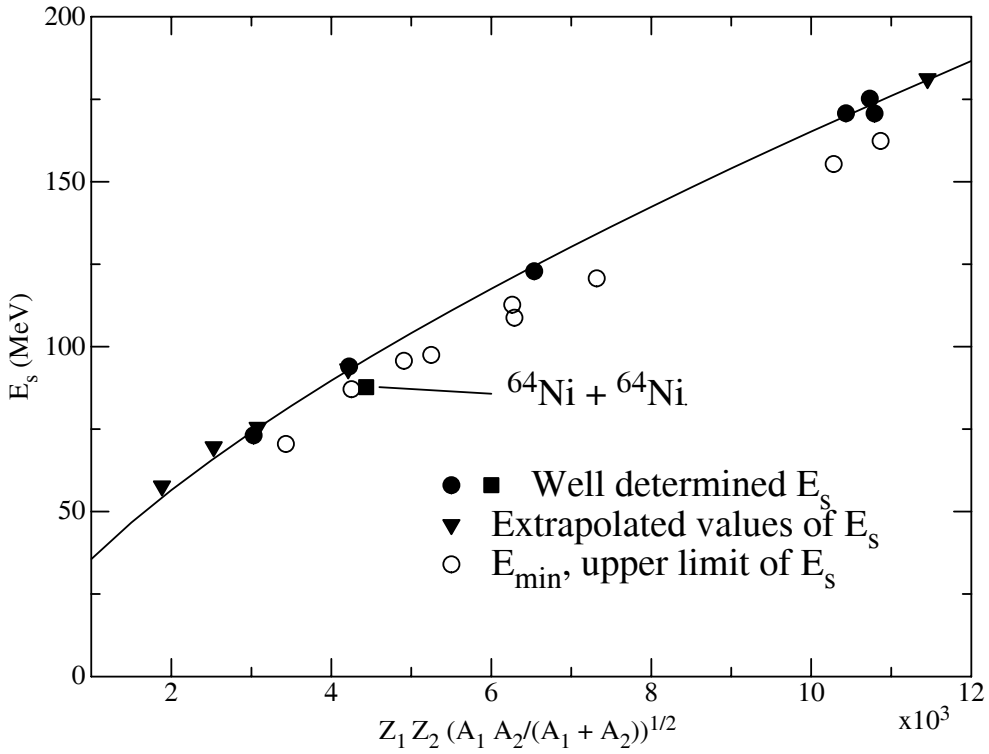

Fig. I-55. Systematics of the energy E_s where the S factor has a maximum as a function of the parameter, $Z_1 Z_2 \sqrt{A_1 A_2 / (A_1 + A_2)}$. The solid curve is calculated with the empirical expression given by Eq. 4. The solid points were obtained for systems that exhibit a clear maximum in the S factor (Category I in Table I-3). The triangles were obtained by extrapolating the logarithmic derivative to the value for a constant S factor, Eq. 2. The open circles show the lowest measured energy, E_{min}, for those systems where no sign of a maximum in the S factor was found so far.

This expression is represented by the solid curve in Fig. I-55. The solid points are the experimental values E_s obtained for the systems of Catagory I. Except for ^{64}Ni + ^{64}Ni, (solid square) all the other systems are well described by the solid line as expected. An important feature of these six systems is that the reacting nuclei are all rather stiff. As for system ^{64}Ni + ^{64}Ni, the L_s value is 2.70 MeV^{-1}, and the E_s point deviates from the curve (Eq. 4), because it is an open-shell system. This will be discussed in another contribution[6] in more detail.

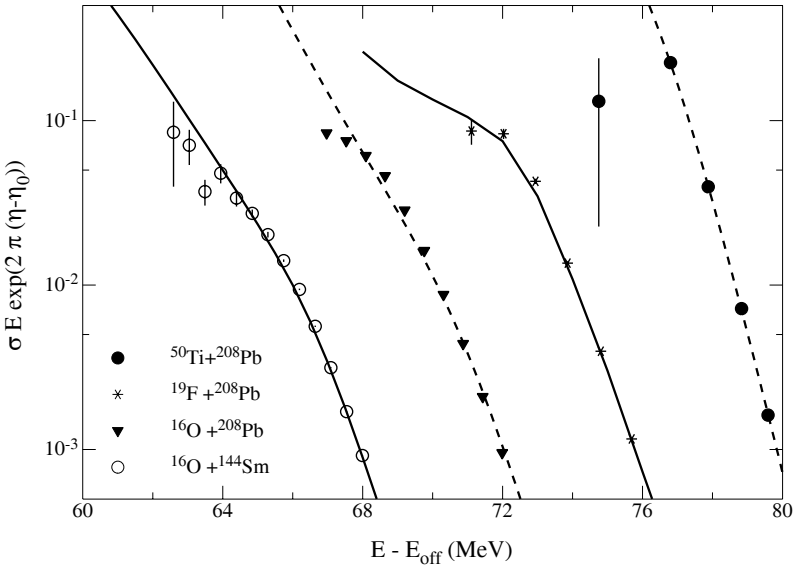

Fig. I-56. Plots of the S factors vs. E - E_{off} for systems where the S factor has not quite developed a clear maximum. The parameters η_0 and E_{off} (MeV) are used to conveniently place many colliding systems on the same plot. The solid curves are results of coupled-channels calculations, and the dashed curves are fits to the fusion data based on Wong's formula. Values of η_0 and E_{off} are: 40.10, -11 for ^{16}O + ^{144}Sm, 48.41, -3 for ^{16}O + ^{208}Pb, 56.30, -3 for ^{19}F + ^{208}Pb, 74.20, 7 for ^{64}Ni + ^{64}Ni, and 126.80, 92 for ^{50}Ti + ^{208}Pb, respectively.

There are other measurements in the literature where the *S* factor has not quite reached a well-defined maximum, but starts to deviate at the lowest energies from the calculations based on the coupled-channels formalism or on Wong's.[8] There is even some evidence for a maximum in one or two cases. Examples are: ^{50}Ti + ^{208}Pb,[9] ^{19}F + ^{208}Pb,[10] ^{16}O + ^{208}Pb,[11] ^{16}O + ^{144}Sm[12] and ^{40}Ca + ^{90}Zr.[13] These systems are included in Table I under Category II, and some are displayed in Fig. I-56. The solid curves represent the coupled-channels calculations reported in the original references. The behavior for ^{16}O + ^{144}Sm and ^{40}Ca + ^{90}Zr at the lowest energies is similar to that seen for ^{90}Zr + ^{90}Zr which, as mentioned in Ref. 1, might be due to small contaminations by heavier isotopes in the target. The triangles in Fig. I-55 are estimated values of E_s obtained by extrapolating the logarithmic derivatives of the measurements to the point where they intersect the curve L_{CS} for a constant *S* factor, defined in Eq. 2. The estimated values of E_s are in reasonable agreement with the solid curve, and they are all rather stiff systems too.

Fusion experiments with "softer" or well-deformed nuclei have usually not been studied at sufficiently low energies which extend into the region where the *S* factor exhibits a maximum. This is not surprising since the strong coupled-channels effects, typical for softer or well-deformed nuclei, tend to broaden the effective barrier distribution[14] and push the energy where the steep rise in the logarithmic derivative occurs to even lower energies. Examples of systems where stronger couplings play a role are: ^{19}F + ^{232}Th,[15] ^{40}Ca + ^{96}Zr,[13] ^{64}Ni + ^{74}Ge,[16] ^{40}Ar + ^{116}Sn, ^{40}Ar + ^{148}Sm, ^{40}Ar + ^{154}Sm,[17] and ^{86}Kr + ^{76}Ge, ^{86}Kr + ^{100}Mo, ^{86}Kr + ^{104}Ru.[18] These systems are included in Table I-3 under Category III. Some of them are shown in Fig. I-57 as well. The open circles in Fig. I-55 are upper limits for the corresponding E_s values and represent the lowest energy where measurements have been performed.

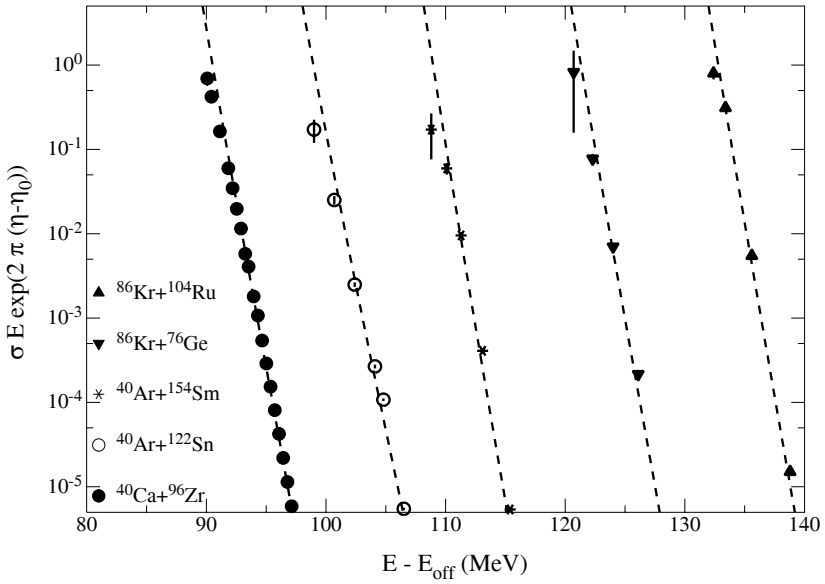

Fig. I-57. Plots of the S factors vs. E - E_{off} for "softer" or well-deformed nuclei systems. The dashed curves are fits to the fusion data based on Wong's formula. Others are the same as in Fig. 2. Values of η_0 and E_{off} are: 72.15, -3 for $^{40}Ca + ^{96}Zr$, 80.16, -5 for $^{40}Ar + ^{122}Sn$, 94.86, 0 for $^{40}Ar + ^{154}Sm$, 104.78, 0 for $^{86}Kr + ^{76}Ge$, and 134.17, 30 for $^{86}Kr + ^{104}Ru$, respectively.

The experimental data referenced in the discussions above and in Ref. 3 are mostly cross sections for fusion-evaporation. For the $^{19}F + ^{208}Pb$[10] and $^{16}O + ^{208}Pb$ reactions[11], total fusion cross sections are available. Fission is the main contributor to fusion for these two systems even at lowest energies. It thus appears that the systematic behavior discussed above is present for both fusion-evaporation and fusion-fission reactions.

To summarize, we have, for fusion reactions with stiff partners, derived a simple empirical formula for the energy where the *S* factor develops a maximum. This parameterization provides also an upper limit for reactions involving softer nuclei.

[1]C. L. Jiang *et al*., Physics Division Annual Report 2002, Argonne National Laboratory, p. 89 (2002).
[2]M. Beckerman *et al.,* Phys. Rev. C **23**, 1581 (1982).
[3]C. L. Jiang *et al*., Phys. Rev. Lett. **89**, 052701 (2002).
[4]C. L. Jiang *et al*., Physics Division Annual Report 2002, Argonne National Laboratory, p. 85 (2002).
[5]J. G. Keller *et al*., Nucl. Phys. **A452**, 173 (1986).
[6]C. L. Jiang *et al*., see this annual report, sec. I.g.6.
[7]A. Mukherjee *et al*., Phys. Rev. C **66**, 034607 (2002).
[8]C. Y. Wong, Phys. Rev. Lett. **31**, 766 (1973).
[9]S. Hofman *et al.,* Z. Phys. **A358**, 377 (1997).
[10]D. J. Hinde *et al*., Phys. Rev. C **60**, 054602 (1999); see also "Proc. the Tours Symposium on Nucl. Phys. III", Tours, France, 1997, AIP Conf. Proc. **425**, 223 (1998).
[11]C. R. Morton *et al*., Phys. Rev. C **60**, 044608 (1999).
[12]J. R. Leigh *et al*., Phys. Rev. C **52**, 3151 (1995); H. Esbensen *et al*., Phys. Rev. C **54**, 3109 (1996).
[13]H. Timmers *et al* ., Nucl. Phys. **A633**, 421 (1998).
[14]N. Rowley, G. R. Satchler, and P. H. Stelson, Phys. Lett. **B254**, 25 (1991).
[15]D. M. Nadkarni *et al*., Phys. Rev. C **59**, R580 (1999).
[16]M. Beckerman et al., Phys. Rev. C **25**, 837 (1982)
[17]W. Reisdorf *et al*., Nucl. Phys. **A438**, 212 (1985).
[18]W. Reisdorf *et al*., Nucl. Phys. **A444**, 154 (1985).

TABLE I-3. The parameter $\varsigma = Z_1 Z_2 \sqrt{A_1 A_2 /(A_1 + A_2)}$, the energy E_s and the logarithmic derivative L_s, that characterize the maximum of the *S* factor for different systems. Also given are the lowest measured energy (E_{min}) and the corresponding cross section (σ_{min}). The first category of systems exhibits a clear maximum in the *S* factor. In the second category, a maximum has not quite been reached, but can be estimated by extrapolating the logarithmic slope to the value for a constant *S* factor. In the third category, there is no clear sign of a maximum in the *S* factor.

System	ζ	E_s (MeV)	L_s (1/MeV)	E_{min} (MeV)	σ_{min} ($\Delta\sigma$) (μb)	Ref.
Category I						
^{58}Ni + ^{58}Ni	4222	94.0	2.29	93.3	49 (20) [2]	
^{60}Ni + ^{89}Y	6537	122.9	2.37	121.4	<0.09	[3]
^{90}Zr + ^{89}Y	10436	170.8	2.31	168.7	0.34 (0.07)	[5]
^{90}Zr + ^{90}Zr	10733	175.2	2.29	172.1	0.08 (0.07)	[5]
^{90}Zr + ^{92}Zr	10792	170.7	2.40	169.6	0.12 (0.05)	[5]
^{32}S + ^{89}Y	3027	73.1	2.40	72.68	60 (20)	[7]
^{64}Ni + ^{64}Ni	4435	87.7	2.70	85.55	<0.005	[4]
Category II						
^{16}O + ^{144}Sm	1882	57.7	2.13	56.6	150 (80)	[12]
^{16}O + ^{208}Pb	2529	69.6	2.15	70.0	240 (10)	[11]
^{19}F + ^{208}Pb	3079	75.5	2.32	75.1	23 (4)	[10]
^{40}Ca + ^{90}Zr	4210	93.2	2.32	93.4	840 (160)	[13]
^{50}Ti + ^{208}Pb	11454	181.2	2.32	179.8	0.00001	[9]
Category III						
^{19}F + ^{232}Th	3394			70.5	0.58 (0.08)	[15]
^{40}Ca + ^{96}Zr	4251			91.7	41 (6)	[13]
^{40}Ar + ^{116}Sn	4908			95.7	3.8 (1.1)	[17]
^{64}Ni + ^{74}Ge	5249			97.5	13.3 (3.3)	[16]
^{40}Ar + ^{148}Sm	6262			112.7	0.8 (0.5)	[17]
^{40}Ar + ^{154}Sm	6289			108.8	1.6 (0.9)	[17]
^{86}Kr + ^{76}Ge	7317			120.7	6.8 (5.5)	[18]
^{86}Kr + ^{100}Mo	10281			155.4	14.4 (1.5)	[18]
^{86}Kr + ^{104}Ru	10868			162.4	4.9 (0.8)	[18]

g.6. Influence of Nuclear Structure on Sub-Barrier Hindrance in Ni + Ni Fusion

(C. L. Jiang, K. E. Rehm, R. V. F. Janssens, H. Esbensen, I. Ahmad, B. B. Back, P. Collon, C. N. Davids, J. Greene, D. J. Henderson, G. Mukherjee, R. Pardo, M. Paul, T. O. Pennington, D. Seweryniak, S. Sinha, and Z. Zhou)

The fusion evaporation excitation function of ^{64}Ni + ^{64}Ni down to the 10 nb level[1] is shown in Fig. I-58. This is the first observation of a maximum in the *S*-factor, which signals a strong sub-barrier hindrance for fusion between two open-shell nuclei. A comparison with the systems ^{58}Ni + ^{58}Ni,[2] ^{58}Ni + ^{60}Ni,[3] and ^{58}Ni + ^{64}Ni,[4] indicates a strong dependence of the energy where this hindrance occurs on the stiffness of the interacting nuclei.

Coupled-channels calculations are fitted to our new data with the nuclear structure input given in Table I-4. The full calculations include 2^+ and 3^- one-phonon excitations, the mutual excitation, and the two-phonon quadrupole excitation estimated within a vibrational model. The result of this calculation is given in Fig. I-58 as a dotted curve in comparison with the experimental data. A modified coupled-channels calculation, which increases the diffuseness parameter inside the barrier to a value a_i while keeping the diffuseness parameter outside the barrier at its original value, was introduced in Ref. 5. A calculation with a_i = 5 fm is given by the solid curve in Fig. I-58. It is evident that the experimental cross sections exhibit a steeper falloff below E_{lab} = 176 MeV than can be accounted for by the coupled-channels calculations.

The experimental logarithmic derivatives, $L(E) = d(ln(\sigma E))/dE$ presented as solid points in Fig. I-59(a), exhibit an increase towards lower energies, which cannot be reproduced by the coupled-channels calculations. The dash-dotted curve in Fig. I-59(a) represents the logarithmic derivative obtained for an *s*-wave transmission of a pure point-charge Coulomb potential or for a constant *S*-factor, which as shown in Ref. 5 is given by

$$L_{CS}(E) = \frac{\pi\eta}{E}, \quad (1)$$

where η is the Sommerfeld parameter. At the lowest energies, all calculated curves are nearly parallel, and are unable to describe the general behavior of the experimental data. This indicates that a substantial component, yet to be identified, is missing in the description of the reaction.

The *S*-factor representation for the ^{64}Ni + ^{64}Ni data (solid points) is shown together with the coupled-channels calculation (using a_i = 5 fm, solid curve) in Fig. I-59(b). A clear maximum of the *S*-factor is observed in the experimental data, but not in the calculation. In Ref. 5, an extrapolated value for the location of the maximum of the *S*-factor, E_s = 89.0 MeV, was obtained using the data of Ref. 6. Based on the present experiment, the measured value is 87.7 MeV, with the difference mainly due to the systematic shift of the two excitation functions (see Ref. 7). This maximum occurs at the crossing point of the experimental logarithmic derivative and the $L_{CS}(E)$ curve. For comparison we show also the *S*-factor for the ^{58}Ni + ^{58}Ni system from Ref. 2. We note that the *S*-factor maximum in the latter case occurs at a significantly higher energy, E_s = 94 MeV. The comparison of these *S*-factor maxima will be discussed further below. It was recently pointed out[5] that the center-of-mass energy, E_s, of the *S*-factor maximum observed in six fusion systems involving "stiff" nuclei is well approximated by

$$E_s^{ref} = 0.355(Z_1 Z_2 \sqrt{\mu})^{2/3}(MeV), \quad (2)$$

where $\mu = A_1A_2/(A_1 + A_2)$ is the reduced mass of the system. This expression corresponds to a value of L_{CS} = 2.34 MeV^{-1}. It is interesting to compare the four systems ^{58}Ni + ^{58}Ni,[2] ^{58}Ni + ^{60}Ni,[3] ^{58}Ni + ^{64}Ni,[4] and ^{64}Ni + ^{64}Ni in order to study the progression from "stiff" to "open-shell" nuclei in the entrance channel. The energies E_s plotted vs. $Z_1Z_2\sqrt{\mu}$ for these four systems are shown in Fig. I-60 The solid circles are for ^{58}Ni + ^{58}Ni and ^{64}Ni + ^{64}Ni, for which E_s values were obtained with an uncertainty of ~1%. The triangles represent the systems ^{58}Ni + ^{60}Ni and ^{58}Ni + ^{64}Ni, for which E_s were obtained by extrapolations of the logarithmic derivative to the crossing point with $L_{CS}(E_S)$. The accuracy of this procedure is estimated to be ~2%. It is evident that the deviation of E_s from E_s^{ref} is related to the neutron number of the colliding nuclei in the entrance channel, which also reflects the stiffness of the systems. For the "soft" ^{64}Ni + ^{64}Ni system the measured value of E_s = 87.7 MeV is about 9% lower than the value of E_s^{ref} = 96.1 MeV, which is expected based on the systematics for "stiff" nuclei. Note that the interaction barrier for these two systems is reduced by only 3%. A similar, but less accurately determined, behavior is observed for the systems ^{16}O + ^{144,148,154}Sm,[8] ^{40}Ar + ^{144,148,154}Sm,[9] and ^{90}Zr + ^{90,92,96}Zr.[10]

In conclusion, we analyzed the fusion excitation function for ^{64}Ni + ^{64}Ni within the coupled channels approach and observed a strong fusion hindrance at extreme sub-barrier energies. In comparison with data for ^{58}Ni + ^{58}Ni, we find that the onset of the sub-barrier fusion hindrance in ^{64}Ni + ^{64}Ni is shifted by 8.4 MeV towards lower center-of-mass energies, whereas a 2 MeV higher energy was expected based on the systematics. This effect appears to be associated with the nuclear structure of the interacting nuclei, with ^{64}Ni being "softer" than ^{58}Ni. At this point there is a clear experimental observation of sub-barrier suppression and of its dependence on the structure of the interacting nuclei. No satisfactory theoretical explanation of this effect was proposed thus far. By measuring the fusion process to ever lower sub-barrier energies, the dependence on the interaction potential at shorter ion-ion distances is being probed in a way that may reveal inadequacies of the present assumptions.[11] Further work, both experimental and theoretical, is required to reach an understanding of this phenomenon.

[1]C. L. Jiang *et al*., Physics Division Annual Report 2002, Argonne National Laboratory, p, 85 (2002).
[2]M. Beckerman *et al*., Phys. Rev. C **23**, 1581 (1982).
[3]A. M. Stefanini *et al*., Phys. Rev. Lett. **74**, 864 (1995).
[4]M. Beckerman *et al*., Phys. Rev. C **25**, 837 (1982).
[5]C. L. Jiang *et al*., Phys. Rev. C **69**, 014604 (2004).
[6]D. Ackermann *et al*., Nucl. Phys. **A609**, 91 (1996).
[7]C. L. Jiang *et al*., see this annual report, sec. I.g.5.
[8]J. R. Leigh *et al*., Phys. Rev. C **52**, 3151 (1995).
[9] W. Reisdorf *et al*., Nucl. Phys. **A438**, 212 (1985).
[10]J. G. Keller *et al*., Nucl. Phys. **A152**, 173 (1986).
[11]C.H. Dasso and G. Pollarolo, Phys. Rev. C **68**, 054604 (2003).
[12]J. Charbonneau *et al*., Bull. Am. Phys. Soc. **16**, 625 (1971).
[13]F. Videbaek *et al*., Nucl. Phys. **A256**, 301 (1976).
[14]M. R. Braunstein *et al.*, Phys. Rev. C **37**, 1870 (1988).
[15]R. A. Broglia and A. Winther, Heavy Ion Reactions (Addison-Wesley, New York, 1991).
[16]H. Esbensen and S. Landowne, Phys. Rev. C **35**, 2090 (1987).

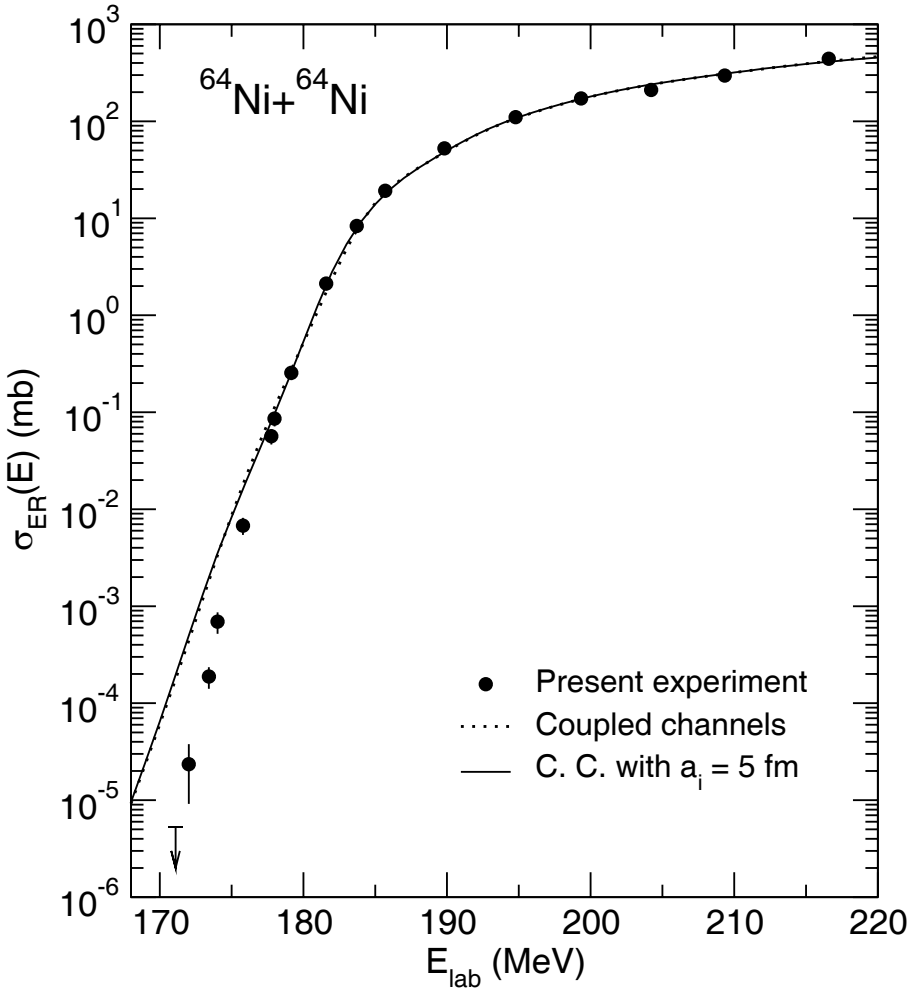

Fig. I-58. Experimental evaporation residue cross sections $\sigma(E)$ (solid circles) plotted as a function of center of mass energy E for the system ^{64}Ni + ^{64}Ni. The dashed and solid curves represent coupled-channels calculations, which are fit to the high energy part of the present data (see text for details).

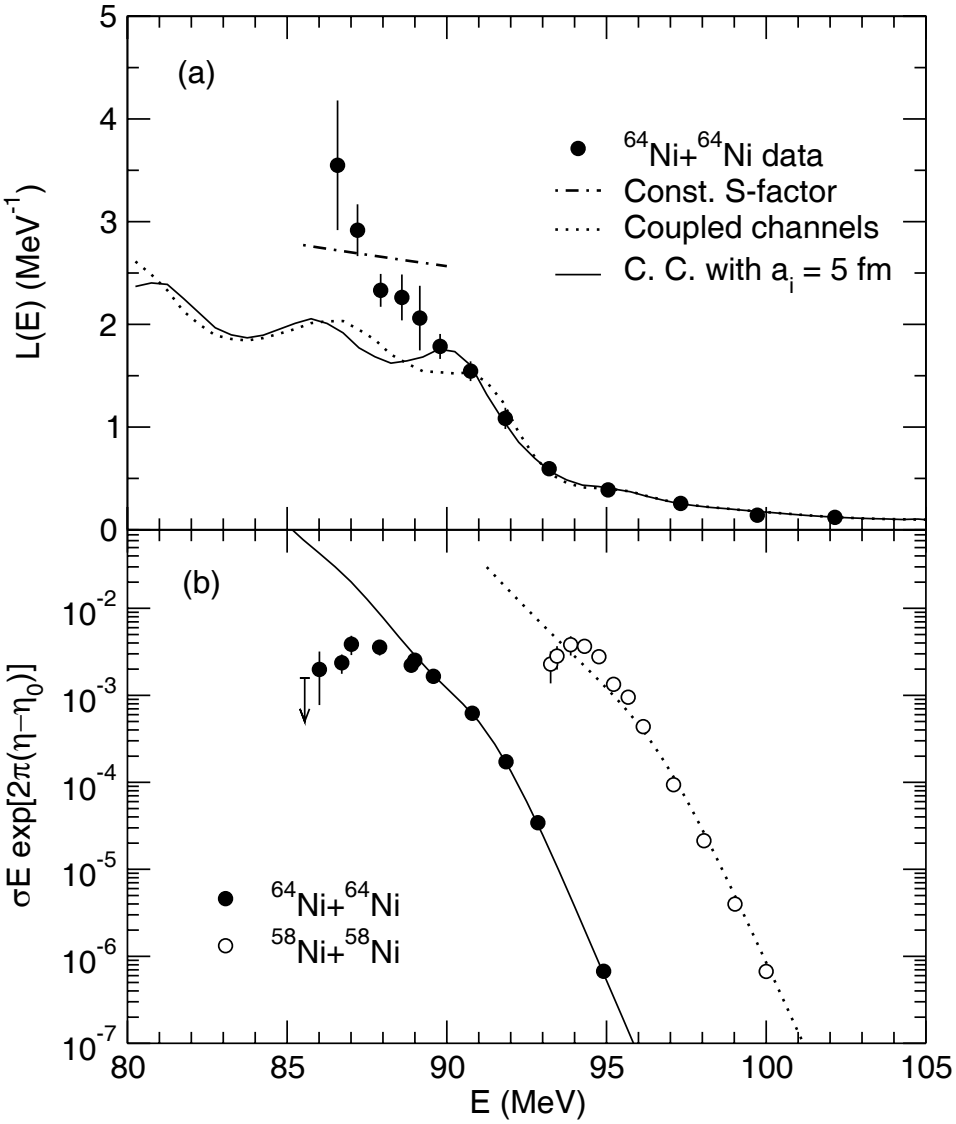

Fig. I-59. (a) The logarithmic derivative L(E) = d(ln σE)/dE plotted as function of center-of-mass energy E. The solid circles were derived from the data by least-squares fits to three consecutive data points. Coupled-channels calculations are shown as the solid and dotted curves, whereas the dash-dotted curve corresponds to a constant S-factor. (b) The S-factor for ^{64}Ni + ^{64}Ni (solid points) is compared to that for ^{58}Ni + ^{58}Ni[2] (open points). The solid curve represents a coupled-channels calculation using a_i = 5 fm for the ^{64}Ni + ^{64}Ni system. The dotted curve is a coupled-channels calculation taken from Ref. 16. The parameter η_0 used to bring different fusion systems onto the same scale are η_0 = 75.23 and η_0 = 69.99 for the ^{64}Ni + ^{64}Ni and ^{58}Ni + ^{58}Ni systems, respectively.

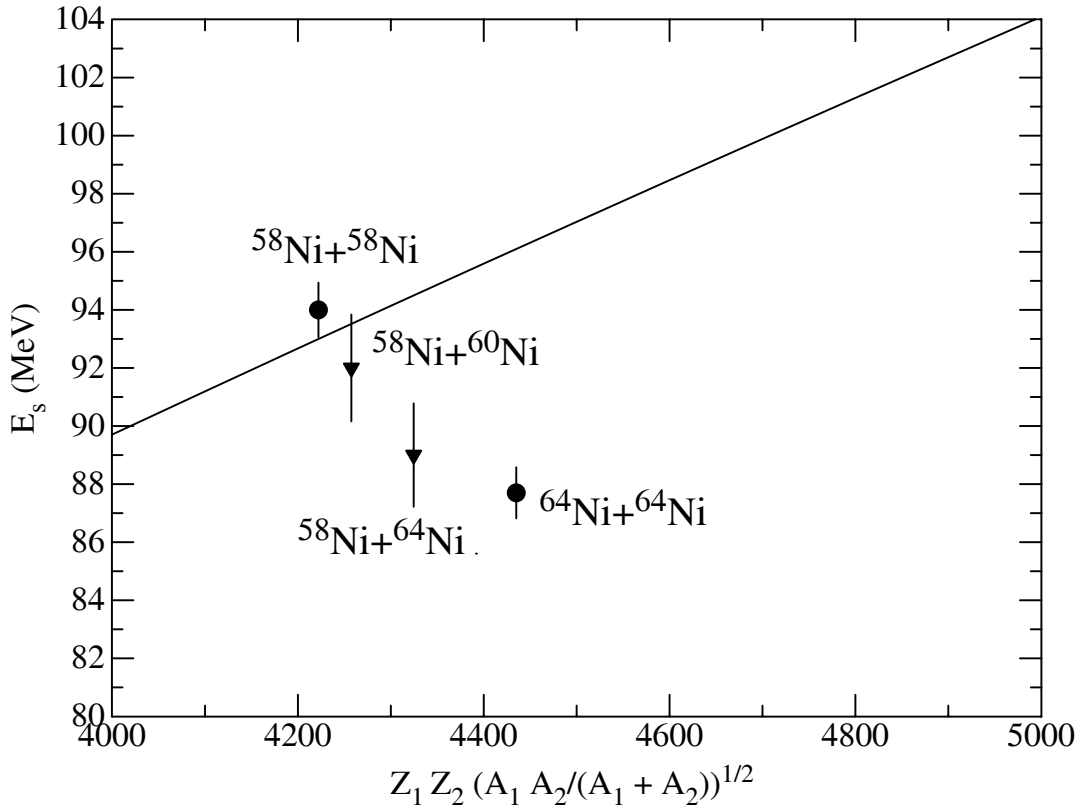

Fig. I-60. Energies E_s plotted vs. $Z_1Z_2\sqrt{\mu}$ for four Ni + Ni systems. For ^{58}Ni + ^{58}Ni and ^{64}Ni + ^{64}Ni, E_s values were obtained with an uncertainty of ~1 %. For the systems ^{58}Ni + ^{60}Ni and ^{58}Ni + ^{64}Ni, E_s were obtained by extrapolations of the logarithmic derivative to the crossing point of $L_{CS}(E_s)$. The accuracy of this procedure is estimated to be ~2%.

Table I-4. Energies and transition probabilities for ^{64}Ni states included in the coupled-channels calculations. The ion-ion interaction parameters used in the calculations are as follows: potential V_0 = 75.98 MeV, diffuseness a = 0.676 fm and radius R = 9.52 fm. Here a radius shift ΔR = 0.10 fm (with reference to the systematic radius)[15] has been adjusted to minimize the χ^2 deviation from the data at high energies.

λ^π	E_χ (MeV)	B(Eλ) ($e^2b^{2\lambda}$)	β_λ^{Coul}	β_λ^{Nucl}
2^+	1.346	650[12]	0.165	0.185[13]
3^-	3.560	20400[14]	0.193	0.200

g.7. A Bragg Scattering Method to Search for the Neutron Electric Dipole Moment

(M. Peshkin, G. R. Ringo, T. W. Dombeck,* H. Kaiser,† D. Koetke,‡ S. Shirvel,‡ R. K. Smither,§ and S. A. Werner¶)

Work is currently focused on a preliminary experiment to measure the neutron magnetic dipole moment (MDM) in the same way that we propose to measure the neutron electric dipole moment (EDM). Polarized neutrons will undergo several hundred Bragg reflections (several thousand in the EDM case) in a slotted crystal we prepared. The rotation of the polarization of the moving neutrons by the crystalline electric field will be measured. The experiment was approved for running at the Missouri University Research Reactor. A beam line has been made ready for instrumentation and equipped with the primary support table needed for the experiment. Devices for transporting, holding, and aligning the crystal were built. The analyzer is in hand and construction of the polarizer is underway. We plan to assemble all of these parts and to mount them inside a solenoid on the table in late spring 2004. Preliminary runs with neutrons are planned for summer 2004, and experimental MDM runs are planned for the remainder of the calendar year.

*University of Hawaii, †University of Missouri, ‡Valparaiso University, §APS User Program Division, Argonne National Laboratory, ¶National Institute of Standards and Technology.